J. Fluid Mech. (2008), *vol.* 613, *pp.* 233–254.
doi:10.1017/S002211200800308X Printed in the United Kingdom

Stochastic forcing of the Lamb–Oseen vortex

J. FONTANE, P. BRANCHER AND D. FABRE

Institut de Mécanique des Fluides de Toulouse (IMFT), Université Paul Sabatier,
2 Allée du Professeur Camille Soula, 31400 Toulouse, France

(Received 27 July 2007 and in revised form 20 June 2008)

The aim of the present paper is to analyse the dynamics of the Lamb–Oseen vortex when continuously forced by a random excitation. Stochastic forcing is classically used to mimic external perturbations in realistic configurations, such as variations of atmospheric conditions, weak compressibility effects, wing-generated turbulence injected into aircraft wakes, or free-stream turbulence in wind tunnel experiments. The linear response of the Lamb–Oseen vortex to stochastic forcing can be decomposed in relation to the azimuthal symmetry of the perturbation given by the azimuthal wavenumber m. In the axisymmetric case $m = 0$, we find that the response is characterized by the generation of vortex rings at the outer periphery of the vortex core. This result is consistent with recurrent observations of such dynamics in the study of vortex–turbulence interaction. When considering helical perturbations $m = 1$, the response at large axial wavelengths consists of a global translation of the vortex, a feature very similar to the phenomenon of vortex meandering (or wandering) observed experimentally, corresponding to an erratic displacement of the vortex core. At smaller wavelengths, we find that stochastic forcing can excite specific oscillating modes of the Lamb–Oseen vortex. More precisely, damped critical-layer modes can emerge via a resonance mechanism. For perturbations with higher azimuthal wavenumber $m \geqslant 2$, we find no structure that clearly dominates the response of the vortex.

1. Introduction

From large hurricanes developing in the atmosphere to the well-known Kelvin–Helmholtz billows in shear layers, vortices are ubiquitous in fluid flows. They are notably major ingredients of turbulence as they are involved in the energy cascade, entrainment and mixing. The understanding of their dynamics is thus of considerable interest. In the context of aeronautics, the need to reduce the aircraft wake and the associated hazards for following planes has motivated the study of the stability of columnar vortices. Since the early works of Crow (1970), Moore & Saffman (1975) and Tsai & Widnall (1976), many studies have shown the sensitivity of the wing-tip vortex pair to both long- and short-wave cooperative instabilities, see Leweke & Williamson (1998) or Billant, Brancher & Chomaz (1999) amongst others. On the other hand, a single vortex is asymptotically stable but it supports various families of oscillating and damped modes amongst which are the so-called Kelvin waves (Fabre, Sipp & Jacquin 2006). Although commonly used, the standard modal stability approach fails to fully predict the vortex linear dynamics; transient growth can occur when specific perturbations are introduced into the flow. Antkowiak & Brancher (2004) have calculated such disturbances for the Lamb–Oseen vortex and found evidence of a core contamination mechanism combining Orr (1907*a*, *b*) and induction effects. The associated energy amplification can reach levels high enough to activate the

nonlinearities and eventually lead to another equilibrium state or trigger a so-called 'bypass' transition to turbulence. In the axisymmetric case, Pradeep & Hussain (2006) (referred to as PH06 in the following) recently found similar transient amplifications. Antkowiak & Brancher (2007) (hereinafter referred to as AB07) completed the picture with the identification of a physical mechanism specific to vortices leading to the generation of vortex rings in the potential region around the vortex core.

The inability of modal analysis to predict such transient energy amplification was previously shown for wall-bounded shear flows, see Butler & Farrell (1992, 1993), Reddy & Henningson (1993) and Farrell & Ioannou (1993*a*). Thus both Couette and Poiseuille plane flows experience energy amplification even in their modal stability domain when subjected to adequate perturbation. The physical mechanism involved consists of the emergence of strong streamwise velocity streaks emanating from streamwise vortices in the flow.

This general occurrence of transient growth in asymptotically stable flows is intimately related to the non-normality of the associated linear dynamical operator (Trefethen *et al.* 1993; Farrell & Ioannou 1994). Let us consider a flow represented by the following dynamical system for the state vector $\boldsymbol{x}$:

$$\frac{\mathrm{d}\boldsymbol{x}}{\mathrm{d}t} = \boldsymbol{A}\boldsymbol{x}, \tag{1.1}$$

where $\boldsymbol{A}$ is the operator corresponding to the Navier–Stokes equations linearized around a given basic state. The base flow is said to be asymptotically stable if all the eigenvalues of $\boldsymbol{A}$ have a negative real part. When the dynamical operator is non-normal, i.e. $\boldsymbol{A}^H\boldsymbol{A} \neq \boldsymbol{A}\boldsymbol{A}^H$ with $(.)^H$ denoting the Hermitian transpose (Farrell & Ioannou 1993*b*, 1994), this approach does not address the issue of the flow energetics for finite times. The stability analysis of a non-normal operator results in a set of modes that decay individually but do not form an orthogonal basis. As a result, one can construct a perturbation on this basis with expansion coefficients that are large but with modes cancelling each other to give an initial energy of order one. Since each eigenmode evolves independently, the initial cancellation may not persist. The energy of the disturbance can thus increase substantially before decaying ultimately to zero. Schmid (2007) gives an illustrative two-dimensional geometric example of this scenario in his recent review on non-modal stability analysis. This mathematical property of non-normal operators reveals of physical mechanisms that lead to transient energy amplification. The lack of orthogonality corresponds to the potential for energy extraction from the basic flow by a subspace of perturbations, leading to transient growth despite the absence of modal (i.e. exponential) instability, a result already pointed out in the seminal work of Orr (1907*a*, *b*).

This characteristics of non-normal operators can be explained in a more formal way by considering the equation governing the instantaneous rate of energy change

$$\frac{\mathrm{d}E}{\mathrm{d}t} = \frac{\mathrm{d}}{\mathrm{d}t}(\boldsymbol{x}^H\boldsymbol{x}) = \boldsymbol{x}^H(A^H + A)\boldsymbol{x}, \tag{1.2}$$

where the energy of the system is defined by $E = \boldsymbol{x}^H\boldsymbol{x}$ in the H_2 norm. Energy growth occurs when the right-hand side of equation (1.2) is positive. This is mathematically equivalent to requiring that a portion of the numerical range of A, defined by $N(A) = \{z \in \mathbb{C}, z = \boldsymbol{x}^H A\boldsymbol{x}, \boldsymbol{x}^H\boldsymbol{x} = 1\}$, lies in the right half-plane (Reddy, Schmid & Henningson 1993). This can be turned into a condition on the spectrum of the energy operator $\mathscr{K} = A^H + A$, since the largest eigenvalue of $\frac{1}{2}\mathscr{K}$, referred to as the numerical

abscissa (Schmid 2007), is the supremum of $\mathrm{Re}[N(A)]$. Transient growth of energy is likely to occur if $\mathscr{K}$ has at least one eigenvalue with a positive real part.

For flows experiencing such transient growth, it is of interest to find the 'most dangerous initial condition' through a process of optimization. It consists of identifying the initial condition that maximizes its energy growth at a fixed time τ. Such a disturbance is referred to as an optimal perturbation. A second optimization can be conducted with respect to time, leading to the optimal time τ_{opt} that defines the most amplified optimal perturbation, often called the global optimal perturbation. In some cases, it is also relevant to look at other disturbances experiencing transient energy amplification. They are termed sub-optimal perturbations. Among them, short-term optimals correspond to optimal perturbations for fixed times $\tau < \tau_{opt}$ (Corbett & Bottaro 2001).

Given the existence of such optimal disturbances in columnar vortices (Antkowiak & Brancher 2004); PH06; AB07), the important point is to know if they can naturally emerge from uncontrolled perturbations as diverse as atmospheric turbulence, background noise in wind tunnel experiments or turbulence generated by aircraft wings. While the potential for substantial transient growth of properly defined initial perturbations certainly exists, recurrent criticisms of optimal perturbation analyses concern the particular structure of these disturbances. These can be quite intricate and unlikely to occur spontaneously in real conditions since there is no apparent mechanism to excite such specific perturbations. This issue is addressed theoretically in the present paper to some extent. The general technique is to linearize the Navier–Stokes equations of small perturbations to a particular mean flow and then to augment these linear dynamics with stochastic forcing, which is uncorrelated in time i.e. 'white noise') and also possibly uncorrelated in space. This general maintained forcing can be interpreted as a crude way to mimic perturbations arising continuously in real transitioning flows due to background turbulence or any kind of uncontrolled (in space and time) ambient fluctuations. But it should be kept in mind that the main objective of the present work is to understand the role played by the transiently growing disturbances found in the previous optimal perturbation analyses when the forcing lacks the bias of any specific forcing function. In that context, while this analysis may not necessarily apply directly to, say, real-life turbulent vortical flows where only certain types of disturbances may be introduced, it will nevertheless give insight into the importance of the physical mechanisms of transient growth uncovered by the previous optimal perturbation analyses.

The associated dynamical equations can be thought of as a system where background noise is regarded as an 'input' and the resulting random velocity field representing the response of the flow as the 'output'. The ratio of the output energy or variance to that of the input noise gives the energy amplification or gain of the system (Schmid 2007). This analysis has been successfully applied to wall-bounded shear flows (Farrell & Ioannou 1993*b*; Bamieh & Dahleh 2001) and to two-dimensional vortices with radial inflow derived from geophysical applications (Nolan & Farrell 1999). In atmospheric sciences this approach is a classical tool of investigation for the prediction of the statistics of meteorological flows such as the long- and short-term deviations of hurricane tracks from that prescribed by the surrounding flow. For instance, Whitaker & Sardeshmukh (1998) used such a stochastic forcing analysis to recover successfully the observed variances of the winter Northern Hemisphere flow (in particular the location and structure of the storm tracks). Not only are these previous works in good agreement with the results from optimal perturbation analyses, pointing to the

robustness of the growth mechanisms uncovered by these analyses, but they are also shown to be complementary to them.

The paper is organized as follows. The stochastic forcing formulation is introduced for any general linear dynamical system in § 2. Then its derivation for the Navier–Stokes equations is considered. The results are presented in § 3, classically ordered by increasing azimuthal wavenumbers. The results are discussed and interpreted in § 4. The paper ends with the conclusions and perspectives in the last section, § 5.

2. Numerical formulation

2.1. *Stochastically driven linear dynamical systems*

The formalism employed in this section is classical in control theory and we only give a brief synopsis of the main steps for completeness. We consider an asymptotically stable linear dynamical system of the form (1.1) under the influence of an external forcing $\boldsymbol{\xi}$. The system of governing equations can be conveniently written in the following state-space form classically used in the control literature (Jovanovic & Bamieh 2005):

$$\frac{\mathrm{d}\boldsymbol{x}}{\mathrm{d}t} = \boldsymbol{A}\boldsymbol{x} + \boldsymbol{B}\boldsymbol{\xi}, \tag{2.1a}$$

$$\boldsymbol{y} = \boldsymbol{C}\boldsymbol{x}, \tag{2.1b}$$

where $\boldsymbol{x}$ is the state vector with initial condition $\boldsymbol{x}_0$ and $\boldsymbol{y}$ is the output vector. The matrices $\boldsymbol{B}$ and $\boldsymbol{C}$ denote the input and output operators. The forcing considered is stochastic in nature and is assumed to be a temporal Gaussian white noise process with zero mean

$$\langle \boldsymbol{\xi} \rangle = \boldsymbol{0}, \tag{2.2a}$$

$$\langle \boldsymbol{\xi}(t)\boldsymbol{\xi}^H(t') \rangle = \boldsymbol{R}\delta(t-t'), \tag{2.2b}$$

where $\langle\ \rangle$ is the ensemble averaging operator and $\boldsymbol{R}$ the spatial covariance matrix. To represent a specific configuration, the matrix $\boldsymbol{R}$ can be implemented with respect to experimental data. In the absence of such information it can be set equal to the identity matrix, i.e. $R_{ij} = \delta_{ij}$, leading to a spatio–temporal Gaussian white noise. Some refinements may be included in the forcing term in order to represent more specific perturbation fields. For instance, the forcing amplitude can peak near the walls to take into account their influence in wind tunnel experiments as done by Jovanovic & Bamieh (2005) for wall-bounded shear flows. Here, we limit the statistical properties of the forcing terms to the above-mentioned ones so as to mimic the most generic free-stream disturbances occurring in real conditions without favouring any particular region of the flow. As claimed by Farrell & Ioannou (1993*b*), this forcing is not intended to reproduce the full complexity of turbulence observed in experiments. Its aim is to retain the essential physics underlying the variance maintained from any external continuous perturbation field. In that sense, the analysis will give insight into the receptivity of the flow without introducing any *a priori* bias through the characteristics of the forcing in the physical or spectral space.

As a response to this forcing, the emerging state $\boldsymbol{y}$ is a stochastic process with second-order statistics given by the covariance matrix

$$\langle \boldsymbol{y}(t)\boldsymbol{y}^H(t) \rangle = \boldsymbol{C} \int_0^t \mathrm{e}^{\boldsymbol{A}(t-s)}\boldsymbol{B}\boldsymbol{B}^H \mathrm{e}^{\boldsymbol{A}^H(t-s)}\mathrm{d}s\ \boldsymbol{C}^H = \boldsymbol{C}\boldsymbol{Q}(t)\boldsymbol{C}^H, \tag{2.3}$$

where $\boldsymbol{Q}(t)$ is referred to as the controllability Gramian. If the dynamical operator $\boldsymbol{A}$ does not vary in time, the system will reach a statistical steady state where the matrix $\boldsymbol{Q}_\infty = \lim_{t\to\infty} \boldsymbol{Q}(t)$ is solution of a Lyapunov equation

$$\boldsymbol{A}\boldsymbol{Q}_\infty + \boldsymbol{Q}_\infty \boldsymbol{A}^H = -\boldsymbol{B}\boldsymbol{B}^H. \tag{2.4}$$

The mean energy corresponds to the variance of the output stochastic process and can be extracted from the covariance, i.e. $\langle E(t)\rangle = \langle \boldsymbol{y}^H(t)\boldsymbol{y}(t)\rangle = \mathrm{trace}[\boldsymbol{C}^H\boldsymbol{Q}(t)\boldsymbol{C}]$. As classically done in the control literature (Zhou, Doyle & Glover 1995; Schmid 2007), this quantity can be interpreted as the H_2-norm of the transfer function $\mathscr{H}(\omega) = \boldsymbol{C}(\mathrm{i}\omega\boldsymbol{I} - \boldsymbol{A})^{-1}\boldsymbol{B}$ associated with the linear system (2.1). To obtain the energy amplification, denoted as $G_\infty = \langle E_\infty\rangle/\langle E_{inp}\rangle$, one has to determine the input energy introduced by the stochastic forcing. It comes from the variance equation

$$\frac{\mathrm{d}}{\mathrm{d}t}\langle E(t)\rangle = \langle \boldsymbol{x}^H(\boldsymbol{A}^H\boldsymbol{C}^H\boldsymbol{C} + \boldsymbol{C}^H\boldsymbol{C}\boldsymbol{A})\boldsymbol{x}\rangle + \langle \boldsymbol{x}^H\boldsymbol{C}^H\boldsymbol{C}\boldsymbol{B}\boldsymbol{\xi}\rangle + \langle \boldsymbol{\xi}^H\boldsymbol{B}^H\boldsymbol{C}^H\boldsymbol{C}\boldsymbol{x}\rangle. \tag{2.5}$$

Using (2.1*b*) and (2.2*b*), the input energy appearing on the left-hand side of (2.5) becomes

$$\langle E_{inp}\rangle = \langle \boldsymbol{x}^H\boldsymbol{C}^H\boldsymbol{C}\boldsymbol{B}\boldsymbol{\xi}\rangle + \langle \boldsymbol{\xi}^H\boldsymbol{B}^H\boldsymbol{C}^H\boldsymbol{C}\boldsymbol{x}\rangle = 2\,\mathrm{trace}[\boldsymbol{B}^H(\boldsymbol{C}^H\boldsymbol{C})^2\boldsymbol{B}]. \tag{2.6}$$

Coherent structures can be extracted from the random flow field resulting from the forcing through the computation of the eigenmodes of the controllability Gramian. The eigenvalue decomposition of $\boldsymbol{Q}_\infty$, known as the Karhunen–Loève (KL) or proper orthogonal decomposition (POD), will provide flow patterns that participate in the response, ordered according to their contribution to the variance of the statistically steady state (Schmid 2007)

$$\boldsymbol{Q}_\infty \boldsymbol{z}^{(p)} = \gamma^{(p)}\boldsymbol{z}^{(p)}. \tag{2.7}$$

These distributions will be referred to as output structures hereinafter. It is also of interest to know which coherent structures from the input noise participate most in the excitation of the system. This issue can be addressed by considering the adjoint dynamical system† $(\boldsymbol{A}^H, \boldsymbol{B}^H, \boldsymbol{C}^H)$ forced with a similar Gaussian white noise. The second-order statistics of the adjoint output stochastic process are contained in the covariance matrix $\boldsymbol{B}^H\boldsymbol{P}(t)\boldsymbol{B}$ where $\boldsymbol{P}(t)$ is the observability Gramian defined as

$$\boldsymbol{P}(t) = \int_0^t \mathrm{e}^{A^H(t-s)}\boldsymbol{C}^H\boldsymbol{C}\mathrm{e}^{\boldsymbol{A}(t-s)}\mathrm{d}s. \tag{2.8}$$

Its long-time value is also solution of a Lyapunov equation

$$\boldsymbol{A}^H\boldsymbol{P}_\infty + \boldsymbol{P}_\infty\boldsymbol{A} = -\boldsymbol{C}^H\boldsymbol{C}. \tag{2.9}$$

Finally, the eigenvalue decomposition of $\boldsymbol{P}_\infty$, called the back Karhunen–Loève decomposition by Farrell & Ioannou (1993*b*), will provide the coherent forcing structures (referred to as input structures in what follows) ranked according to their contribution to the system excitation

$$\boldsymbol{P}_\infty\boldsymbol{\zeta}^{(p)} = \beta^{(p)}\boldsymbol{\zeta}^{(p)}. \tag{2.10}$$

† A specific notation, say $\boldsymbol{A}^+$, should have been used for the adjoint operator as its definition strictly depends on the chosen inner product. In the present case the adjoint operator $\boldsymbol{A}^+$ is the same as the Hermitian transpose $\boldsymbol{A}^H$ since the standard inner product of the Hilbert space $\mathscr{H}$ with identity weighting is used (Hoepffner 2006).

2.2. *Stochastic forcing applied to Navier–Stokes equations*

The base flow considered in this paper is the Lamb–Oseen vortex. Its non-dimensional azimuthal velocity field is

$$V(r) = \frac{1}{r}(1 - \mathrm{e}^{-r^2}), \tag{2.11}$$

where the characteristic scales used are the vortex dispersion radius r_0 and the angular velocity at the axis Ω_0. In the following, $\Omega(r) = V(r)/r = (1 - \mathrm{e}^{-r^2})/r^2$ and $Z(r) = (1/r)\partial_r(rV(r)) = 2\mathrm{e}^{-r^2}$ represent respectively the angular velocity and the axial vorticity of the columnar vortex. We now consider infinitesimal disturbances expanded in a modal form

$$[\hat{u}_r, \hat{u}_\theta, \hat{u}_z, \hat{p}\,](r, \theta, z, t) = [u, v, w, p\,](r, t)\mathrm{e}^{\mathrm{i}m\theta + \mathrm{i}kz} + \text{c.c.}, \tag{2.12}$$

where c.c. stands for the complex conjugate, m is the azimuthal wavenumber and k the axial wavenumber. The linearization of the incompressible Navier–Stokes equations gives the following set of equations:

$$\frac{1}{r}\partial_r(ru) + \frac{\mathrm{i}m}{r}v + \mathrm{i}kw = 0\,, \tag{2.13a}$$

$$\partial_t u + \mathrm{i}m\Omega u - 2\Omega v = -\partial_r p + \frac{1}{Re}\left[\left(\Delta_{m,k} - \frac{1}{r^2}\right)u - \frac{2\mathrm{i}m}{r^2}v\right], \tag{2.13b}$$

$$\partial_t v + \mathrm{i}m\Omega v + Zu = -\frac{\mathrm{i}m}{r}p + \frac{1}{Re}\left[\left(\Delta_{m,k} - \frac{1}{r^2}\right)v + \frac{2\mathrm{i}m}{r^2}u\right], \tag{2.13c}$$

$$\partial_t w + \mathrm{i}m\Omega w = -\mathrm{i}kp + \frac{1}{Re}\Delta_{m,k}w\,, \tag{2.13d}$$

where the Reynolds number is $Re = \Omega_0 r_0^2/\nu = \Gamma/(2\pi\nu)$ and

$$\Delta_{m,k} \equiv \partial_{rr} + \frac{1}{r}\partial_r - \frac{m^2}{r^2} - k^2. \tag{2.14}$$

The set of variables is reduced to the three velocity components by eliminating the pressure with the Poisson equation. The state variables correspond to the primitive ones, i.e. $\boldsymbol{x} = [u, v, w]$, and both the input and output operators $\boldsymbol{B}$ and $\boldsymbol{C}$ of § 2.1 simply reduce to the identity operator. A Chebyshev spectral collocation method with an algebraic mapping identical to that described by Fabre & Jacquin (2004) and Fabre *et al.* (2006) is used for the spatial discretization of the problem. The energy of the perturbation, which defines a weighted inner product, is defined classically by

$$E = (\boldsymbol{x}, \boldsymbol{x})_E = \frac{1}{2}\int_0^\infty (u^*u + v^*v + w^*w)r\,\mathrm{d}r, \tag{2.15}$$

where $*$ denotes the complex conjugate. The use of the energy-based inner product requires a coordinate transform to convert the statistics measures into the more standard Hermitian H_2 norm (Hoepffner 2006; Schmid 2007). From the Choleski factorization of the symmetric definite positive weight operator $\boldsymbol{W} = \boldsymbol{M}^H\boldsymbol{M}$, the relation between the two norms is $\|\boldsymbol{x}\|_E = \|\boldsymbol{M}\boldsymbol{x}\|_2$ and $\|\boldsymbol{A}\|_E = \|\boldsymbol{M}\boldsymbol{A}\boldsymbol{M}^{-1}\|_2$.

The calculations are carried out with MATLAB using the DMSuite package developed by Weideman & Reddy (2000). The convergence of the numerical procedure depends on both the truncation level N and the radial domain extent r_{max}. We tested the sensitivity of the results to both parameters, and converged calculations were obtained for $N \in [150, 300]$ and $r_{max} \in [5000, 20000]$.

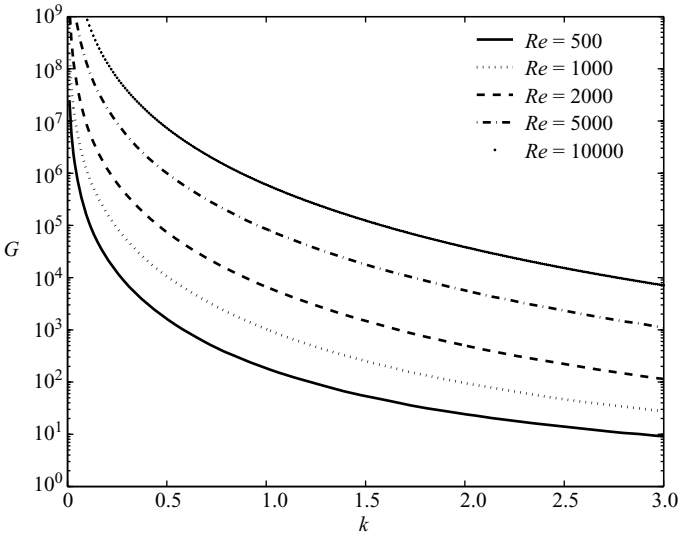

FIGURE 1. Energy amplification for the statistical steady state in the axisymmetric case ($m = 0$) as a function of the axial wavenumber k for various Reynolds numbers.

3. Results

3.1. *The axisymmetric case* ($m = 0$)

The presentation of the results starts with the axisymmetric case. Figure 1 shows the energy amplification as a function of the axial wavenumber for Reynolds numbers varying from 500 to 10000. As in optimal perturbation analyses (PH06, AB07), high levels of amplification are observed. The plot also confirms that the largest amplifications occur for small axial wavenumbers. The amplification levels reach higher values than those found by optimal perturbation analyses, which can be easily understood since the system is excited by a constant input and not solely by an initial condition (Bamieh & Dahleh 2001). This difference in the level of amplification between these two approaches is systematic.

For the $k = 1$ case, we consider the hierarchy of both the input and output structures according to their contribution to the sustained variance of the steady state. The spectra resulting from the eigenvalue problems (2.7) and (2.10) are plotted in figure 2. The energy amplification essentially results from the contribution of the few first structures as the eigenvalues rapidly decrease to negligible values. The first input structure is responsible for 62 % of the vortex excitation and dominates the forcing field. In the same manner, the first ouput structure prevails in the vortex response by contributing to 61 % of the variance sustained by the flow. Figure 3 gives the spatial distribution of these two dominant structures. They are very similar to the optimal perturbation at initial and optimal times found in the optimal perturbation analyses of PH06 and AB07. The forcing structure consists of azimuthal velocity streaks located in the quasi-potential region in the outer periphery of the vortex. The physical mechanism leading to the azimuthal vortex rings of figure 3(b) has been explained by AB07. It has been called 'anti-lift-up' in reference to the so-called 'lift-up' mechanism occurring in planar shear flows, though it is radically different in nature. Briefly, the azimuthal velocity streaks induce a local Coriolis force field yielding a radial displacement of the fluid particles. Its potential part is balanced by the pressure gradient to ensure flow incompressibility. Its rotational part feeds the tori of

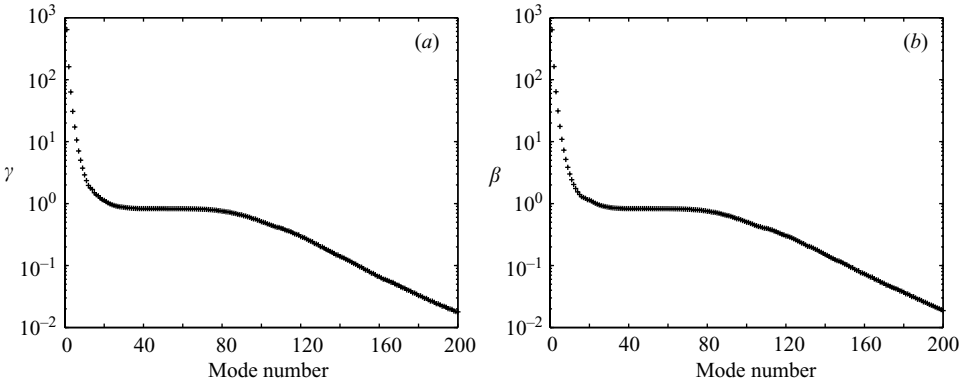

FIGURE 2. Contribution of (*a*) the output structures and (*b*) the input structures to the excitation of the system. The case shown corresponds to $m = 0$, $k = 1$ and $Re = 1000$.

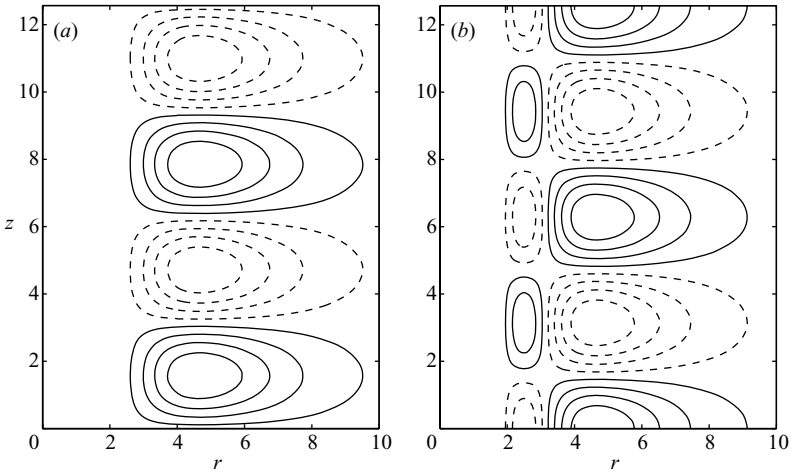

FIGURE 3. Structure of (*a*) the first input (forcing) function (isocontours of azimuthal velocity) and (*b*) the first output (response) function (isocontours of azimuthal vorticity) for $m = 0$, $Re = 1000$ and $k = 1$. Eight equally spaced levels are displayed and dashed contours correspond to negative values.

azimuthal vorticity that constitute the vortex response displayed in figure 3(*b*). AB07 established this original mechanism with the assumption of zero base vorticity. This is a good approximation since the velocity streaks are localized in the quasi-potential region of the base flow. The main trends are correctly captured by this scenario. Nevertheless, the residual base vorticity in the outer periphery of the Lamb–Oseen vortex is at the origin of a small deviation from this idealized view when approaching the vortex core. One can identify weak secondary rolls in figure 3(*b*) located closer to the vortex core. Antkowiak (2005) showed that they are the signature of waves generated in the region of non-zero epicyclic frequency of the basen flow κ defined by $\kappa(r)^2 = 2\Omega(r)Z(r)$ (Rayleigh discriminant). Mathematically, this comes from the coupling term associated with the base vorticity $Z(r)$ in the equation for the azimuthal velocity, see (2.13*c*).

On varying the axial wavenumber, the radial location of both the azimuthal velocity streaks and the resulting azimuthal vortex rings increases with increasing

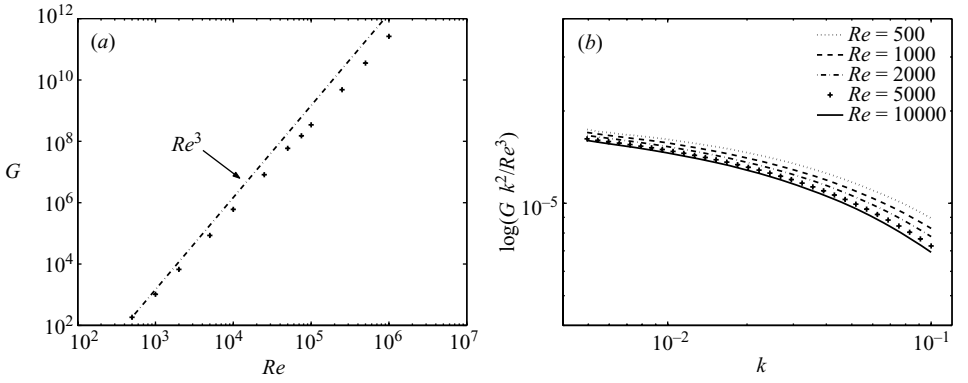

FIGURE 4. (*a*) Influence of the Reynolds number on the energy amplification factor for $k = 1$ and $m = 0$. The cross symbols represent calculations and the dashed-dotted line is the theoretical scaling derived from Antkowiak (2005). For this axial wavenumber, the linear regression from the numerical data gives a gain scaling as $G_\infty = O(Re^{2.77})$. (*b*) Scaling law for small k.

wavelengths (data not shown). This is in agreement with the results of PH06 who related the increasing radial position of the optimal perturbation (and consequently the associated optimal time) with increasing k to the radial distribution of the vorticity-to-strain ratio in the base flow. The anti-lift-up mechanism is observed to dominate the flow dynamics even more as the axial wavenumber decreases. The contribution of the dominant structures to the variance of the response is found to shrink at large k. For $k = 0.1$, the output (resp. input) structure accounts for 78 % (resp. 79 %) of the energy amplification, whereas for $k = 2.5$ the output (resp. input) structure only accounts for 32 % (resp. 32 %) of the gain.

The next point to be discussed is the influence of the Reynolds number. From figure 1, it is obvious that larger Reynolds numbers result in larger energy amplifications by the flow. This is not surprising because of the energy balance between the extraction of energy from the background flow by the stochastic forcing, on the one hand, and the viscous dissipation on the other hand. When looking more precisely at the Reynolds number dependence for the sustained variance, one can obtain a scaling law from a sufficient number of calculations, see figure 4(*a*) for $k = 1$. For the range of axial wavenumbers explored here, the scaling was always found to be of the form $G_\infty = O(Re^\alpha)$ with α decreasing from 3 for $k = 0.1$ to 2.5 for $k = 3$. Antkowiak (2005) showed that an $O(Re^2)$ scaling for the transient energy growth is an upper bound. In the present study, the system is being continuously excited and the energy accumulates before it dissipates. The characteristic diffusion time is $O(Re)$. Hence, the upper bound for the energy growth is $O(Re^3)$ here, which is consistent with the results obtained. This scaling has been derived with the hypothesis of zero base vorticity. The deviation from the predicted scaling law is explained by the existence of the radially propagating waves mentioned previously, which are responsible for an outward radiation of energy (Antkowiak 2005). This point also sheds light on the variation of the exponent α with k in the scaling law found in this study. As k is decreased, the input structures are located further away from the core where the zero base vorticity assumption is more accurate (PH06; AB07). Hence for small wavenumbers there is no wave generation and the scaling law in $O(Re^3)$ becomes exact.

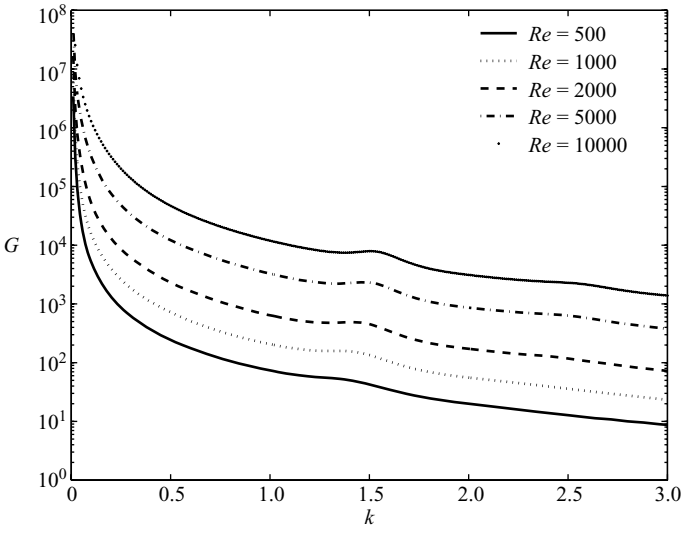

FIGURE 5. Energy amplification in the helical case ($m = 1$) as a function of the axial wavenumber k for various Reynolds numbers.

In addition, variation of the viscous diffusion does not affect the spatial structure of forcing and response. The velocity and vorticity distributions displayed in figure 3 remain unchanged when the Reynolds number is varied. The only difference is in the peaks of both azimuthal velocity and vorticity that rise to higher values when the Reynolds number is increased. Finally, we also obtained an empirical scaling law for the energy amplification when k goes to zero. We found numerically that the gain roughly scales as $O(Re^3/k^2)$ as can be seen in figure 4(b).

3.2. *The helical case* ($m = 1$)

Figure 5 displays the energy gain for the $m = 1$ helical waves as a function of the axial wavenumber for different Reynolds numbers. Compared to the optimal perturbation analyses of Antkowiak & Brancher (2004) and PH06, similar global trends are retrieved and large amplification levels are found. The large increase of the gain for small k is observed as well as the peak around $k = 1.5$ and an emerging one at $k = 2.5$, although less pronounced than in the optimal perturbation analysis of Antkowiak & Brancher (2004). The latter point suggests that the dominant structure does not emerge strongly in the vortex response for this range of wavenumber. This is confirmed quantitatively since the first output structure only contributes 32 % of the sustained variance for $k = 1.35$ and $Re = 1000$. This is the consequence of the coexistence of several perturbations participating in the energy amplification when the system is stochastically forced. For $k = 1.35$, the second emerging structure contributes 11 % to the gain. Hence, the vortex response to the forcing will be dominated by the first output structure. Its axial vorticity is plotted in figure 6 as well as the axial vorticity of the input structure that mainly excites it. This forcing structure is composed of a pair of left-handed spiralling vorticity sheets similar to the initial shape of the optimal perturbation found by Antkowiak & Brancher (2004). These two folded vorticity layers located in the quasi-potential region of the flow are of alternate sign. Their respective velocity inductions on the vortex core initially cancel each other. As time evolves, they progressively uncoil via an Orr mechanism induced by the base-flow differential rotation. Through this process, the reorganization of

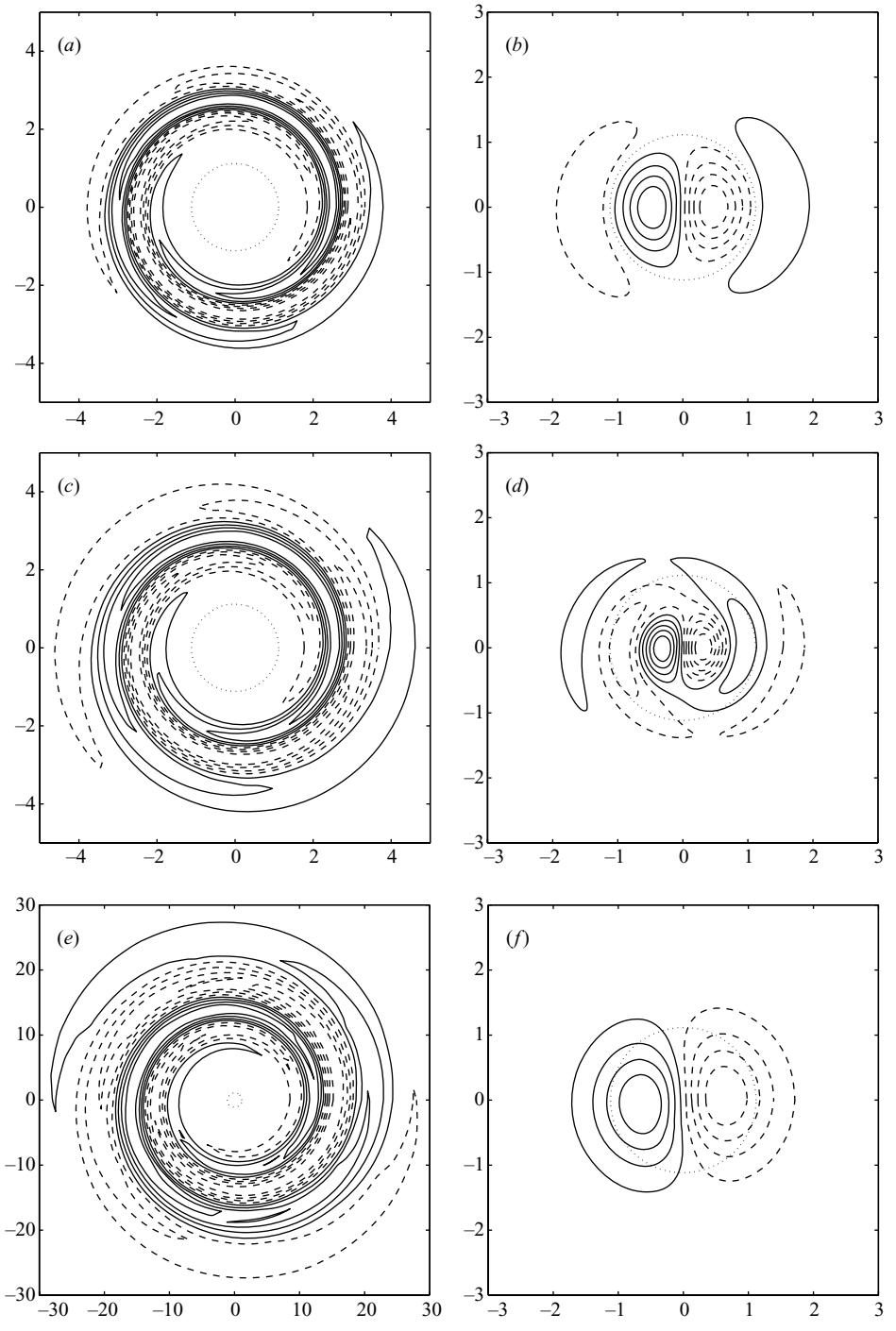

FIGURE 6. Isocontours of axial vorticity for the dominant structures for $m = 1$ and $Re = 1000$. The same convention as in figure 3 is used except for (d) where ten equally spaced levels have been used. The dotted circle corresponds to the location of the maximum azimuthal velocity of the Lamb–Oseen vortex at $r = 1.1209 r_0$. First input structure for (a) $k = 1.35$ accounting for 31 % of the energy amplification, (c) $k = 2.5$ and 17 %, (e) $k = 0.5$ and 50 %. First output structure for (b) $k = 1.35$ accounting for 32 % of the flow excitation, (d) $k = 2.5$ and 16 %, (f) $k = 0.5$ and 52 %.

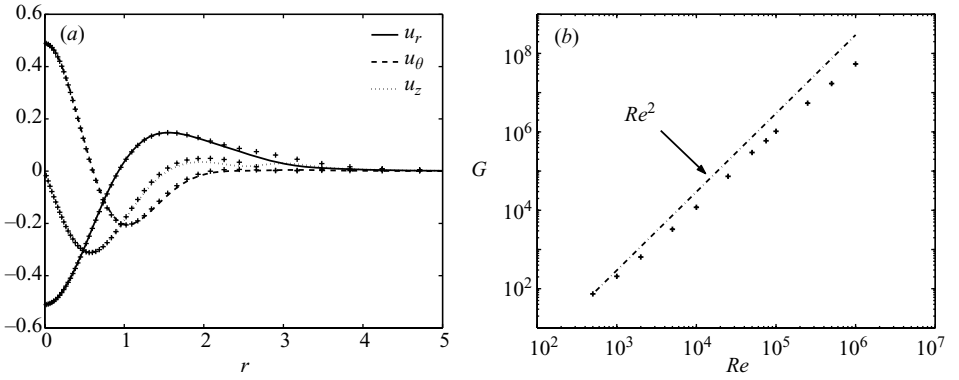

FIGURE 7. (*a*) Comparison of the velocity radial profiles between the first L1 mode of Fabre *et al.* (2006) and the output structure emerging from the stochastic forcing for $k = 1.35$ and $Re = 1000$. The solid, dashed and dotted lines correspond respectively to the radial, azimuthal and axial velocity of the L1 wave. The cross symbols denote the velocity profiles of the output structure. (*b*) Influence of the Reynolds number on the energy amplification factor for $k = 1$ and $m = 1$. The cross symbols represent calculations and the dashed-dotted line the theoretical scaling derived from Antkowiak (2005). For this axial wavenumber, the linear regression from the numerical data gives a gain scaling as $G_\infty = O(Re^{1.8})$.

the vorticity sheets promotes an increasing velocity induction in the vortex core that leads to the emergence of the dominant output structure of figure 6(*b*). This response corresponds to the first critical-layer mode of Fabre *et al.* (2006) as can be seen from the comparison of the velocity radial profiles in figure 7(*a*).

This phenomenon can be interpreted as a transient resonance mechanism: a Kelvin wave of the Lamb–Oseen vortex is excited by the perturbation field induced by the uncoiling of the initial vorticity spirals. This conjecture was first confirmed by Antkowiak (2005) who made a successful comparison with an elementary model of a forced harmonic oscillator. Choosing an adequate forcing term so as to correctly reproduce the influence of the spiralling vorticity arms, the frequency of the forcing term is found to fit very well those of the selected waves. PH06 performed a similar analysis on a top-hat (Rankine) vortex. Their results supported the hypothesis of a resonance-driven excitation of vortex waves. From the simple harmonic oscillator model, one can obtain an expression for the energy gain at large time when the forcing term has a constant amplitude: $G_\infty = 1/(s^2 + (\omega_f - \omega)^2)$ where ω_f is the pulsation of the forcing term, ω the pulsation of an eigenmode of the system and s its damping rate. From this first estimation of the energy growth, one can see that the selection process is based on two criteria. The first consists of selecting one of the least damped waves – minimizing the s term – since it allows a maximal energy amplification. For the present set of parameters, the first critical layer mode – referred to as the first L1 mode according to the nomenclature of Fabre *et al.* (2006) – has the minimum damping rate, see their figure 6. As a consequence it is found to be the dominant output structure. Secondly, the disturbance may be in phase with the wave in order to impose a continuous excitation – minimizing the $(\omega_f - \omega)$ term. This implies that the rotation rate of the spirals is close to the pulsation of the mode. In the quasi-potential region of the flow, the rotation rate of the vorticity sheets is $\Omega(r) \approx 1/r^2$. Hence, the radial position of the spiralling vorticity sheets is imposed by the mode frequency, i.e. $r \approx 1/\sqrt{\omega}$ where ω is the wave pulsation, a criterion previously established by PH06 with the top-hat vortex model (see their figure 21*c*). For the $k = 1.35$ case, the first

L1 wave frequency is 0.121, which gives a mean radial position of $r = 2.9$. This is consistent with the location of the spiral arms in figure 6(*a*).

Keeping in mind these two criteria for the resonance phenomenon and considering the stability results of Fabre *et al.* (2006), it is expected that the mode selection depends on the axial wavenumber. For larger wavenumbers, we found the second L1 mode as the first output structure, see figure 6(*d*) for $k = 2.5$. When k is decreased, the emerging structure displayed in figure 6(*f*) is also of a different nature and corresponds to the displacement wave of the Lamb–Oseen vortex (referred to as the D wave in the following). According to the criteria previously mentioned, the emergence of the D mode is not linked to an exact resonance. This wave being countergrade, i.e. its pulsation is negative, no disturbance can have a similar rotation rate. In this case, the D wave emerges only because its damping rate is very small compared to those of the waves of the L family. It is noteworthy that the spiralling input structure is located far from the vortex core, at a mean radial position $r \approx 15$. This represents a slow time-rotating disturbance with an associated rotation rate $\Omega(r) \approx 0.0044$. This point is linked to the fact that the displacement wave emergence corresponds to an exact resonance in the two-dimensional limit for a steady forcing. For $k = 0$, the D wave is stationary and the exciting perturbation can satisfy the in-phase condition if the spiral arms of vorticity are pushed outwards to an infinite radial position. Obviously, this could not be verified numerically, but we found that the radial location of the input structure increased on reducing the axial wavenumber from $k = 0.5$ to $k = 0.1$. This exact resonance comes with an infinite energy growth as revealed by the large increase of the gain when k goes to zero in figure 5.

The emergence of the displacement wave under continuous external perturbations is a good candidate for explaining the vortex meandering (or wandering) phenomenon. The nature of the wave, namely a long-wavelength bending wave, is in agreement with the characteristics of the meandering observed in wind tunnel experiments (Baker *et al.* 1974; Devenport *et al.* 1996). The theoretical approach used here, which takes into account the external disturbances in the form of a continuous random forcing, is consistent with real experimental conditions where background noise is constantly exciting the wing-tip vortex. This point should be confirmed experimentally by controlling, or at least quantifying, the perturbation field and by correlating the data with measurements of the vortex response. Here we only give a physical mechanism that could explain the occurrence of this phenomenon. But we are still far from a comprehensive and fully predictive description that could help experimentalists to filter out this erratic core displacement. To our knowledge, the best way to proceed is proposed by Devenport *et al.* (1996), who used a Gaussian model for the fluctuations of the vortex core position.

The effect of viscosity has been explored numerically and a general power law has been obtained for the energy amplification, see figure 7(*b*) for $k = 1$. For the range of axial wavenumbers considered here, we found the scaling $G_\infty = O(Re^{1.8})$. This exponent is considered valid for any k since very small variations were observed, i.e. 1.8 ± 0.02. Antkowiak (2005) showed that the transient energy growth is $O(Re)$ for the resonance phenomenon while it is $O(Re^{2/3})$ when only the Orr mechanism is active. Following the same reasoning as in the axisymmetric case, the theoretical upper bound for energy amplification under stochastic forcing is $O(Re^2)$. The results obtained here are in good agreement with this scaling law. A decrease in viscous diffusion also affects the structures. While the vorticity distribution of the Kelvin waves remains practically unchanged, the spiral arms of the dominant disturbance become thinner as the Reynolds number increases, a point already noticed by PH06. The peaks of

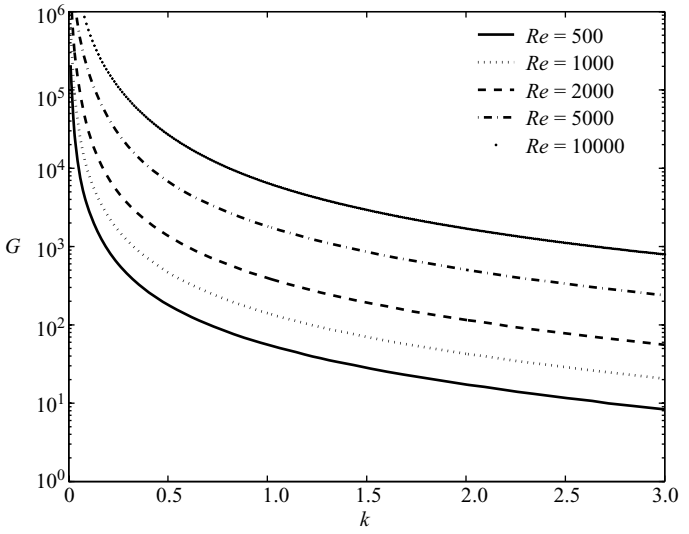

FIGURE 8. Energy amplification reached for the statistical steady state in the double-helix case ($m = 2$) as a function of the axial wavenumber k for various Reynolds numbers.

vorticity also reach larger values, which leads to a stronger velocity induction in the core when the spirals unfold and a higher level of energy amplification.

3.3. *The double-helix case* ($m = 2$) *and higher azimuthal wavenumbers*

The energy gain of the vortex in response to double-helix perturbations is plotted versus the axial wavenumber in figure 8 for different Reynolds numbers. The levels of amplification are lower than in the axisymmetric case but with similar tendencies. For a given Reynolds number, the larger the wavelength the larger the amplification. These results are noticeably different from those of the optimal perturbation analysis (PH06). Not only are the levels much higher but the dependence on k is completely different. The amplification maximum occurs for small wavenumbers and the curve does not present the flat-shaped aspect displayed in figure 19(b) of PH06. The difference in the results can be explained by two complementary arguments. First, the development of the optimal perturbation is completed within few rotation periods of the vortex (Antkowiak 2005). In this case, the transient energy growth of the optimal perturbation may occur on too short a time scale, compared to the statistical mean time between two consecutive excitations of the mode by the external forcing, for being efficiently amplified. After excitation of the vortex with the optimal disturbance extracted from the random noise, the process of energy amplification and decay is likely to be over before another excitation happens. Hence, the energy gain resulting from successive excitations is statistically unlikely to cumulate. As a result, the optimal perturbation will be less amplified under a random forcing than a disturbance associated with a less efficient transient mechanism but occurring on a longer time scale. This point is related to the second argument: strong sub-optimal perturbations competing with the optimal one may exist. They can eventually dominate the response of the vortex when subjected to stochastic maintained forcing if they develop on a larger time scale than the optimal one. Evidence for this conjecture can be obtained by looking at both the input and output structures.

The structures that dominate the input forcing consist of the same kind of spiralling structures as the ones identified in the $m = 1$ helical case (figure 9). The resonance

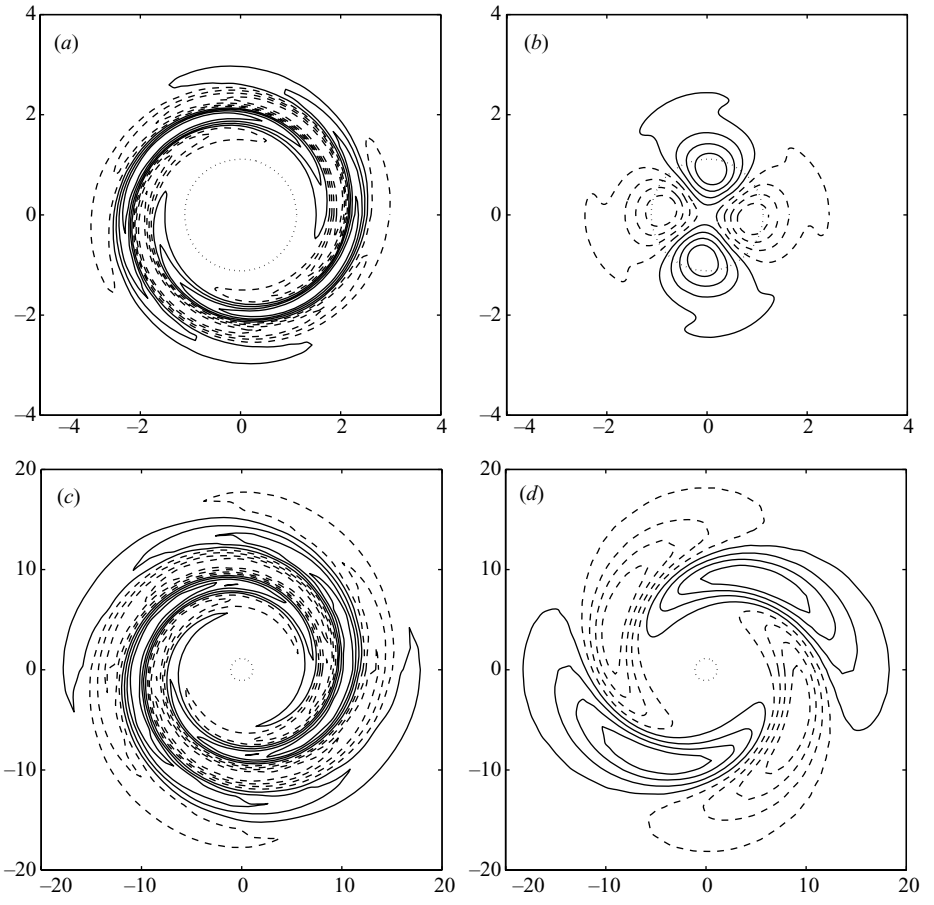

FIGURE 9. Isocontours of axial vorticity for the first functions for $m = 2$ and $Re = 1000$. The same convention as in figure 3 is used. First input structure for (*a*) $k = 2.5$ accounting for 8 % of the energy amplification, (*c*) $k = 1$ and 10 %. First output structure for (*b*) $k = 2.5$ accounting for 8 % of the flow excitation, (*d*) $k = 1$ and 10 %.

mechanism leading to the selection of a Kelvin wave is active and the first output structure for $k = 2.5$, displayed in figure 9(*b*), corresponds to the flattening wave of Fabre *et al.* (2006). This mode being by far the least damped, it is selected on frequency grounds according to the criteria mentioned in the previous section. The mean radial position of the entangled vorticity spirals is imposed by the pulsation of the mode. However, while active, the resonance no longer dominates the flow dynamics since the first input structure accounts for only 8 % of the sustained variance in this case. The sub-optimals participate equally in the excitation of the vortex. For smaller wavenumbers, transient resonance is not even the dominant mechanism leading to energy amplification. Figure 9(*d*) shows the first output structure for $k = 1$. The vortex response is only composed of the four initial vorticity sheets that have been uncoiled. In this case, the Orr mechanism gives the largest energy growth and accounts for 10 % of the total amplification. The spiralling vorticity arms of the input structure are located far from the vortex core so that the time scale of the Orr mechanism is long enough to be efficiently amplified by the stochastic forcing. Its time scale is given

by the duration of the uncoiling of the vorticity arms, which is roughly evaluated by

$$\tau_{\mathrm{Orr}} \approx -\frac{2\pi}{e\partial_r \Omega(r_h)}, \tag{3.1}$$

where e and r_h are respectively the mean width and the radial position of the spiral arm. For the perturbation plotted in figure 9(c), τ_{Orr} is found to be about 50 rotation periods of the vortex, which is one order of magnitude larger than the optimal time. As previously argued, this energy growth mechanism is activated on a longer time scale than the transient resonance, and it is more efficiently amplified by the maintained forcing. Inspection of the less dominant structures reveals that the flattening wave is the fourth preferred response of the flow, accounting only for 4 % of the variance. For the $m = 2$ case, there is no structure that clearly dominates the flow response, by contrast to what has been found for the $m = 0$ and $m = 1$ cases. Whatever the axial wavenumber, the contribution of the most dominant output structure never exceeds 15 %.

Finally, our survey ends with a description of the vortex response for higher azimuthal wavenumbers. We explored the flow behaviour under a continuous stochastic forcing for m as large as 10 and always found energy amplification. The observed gain levels decrease with increasing m and are far below those of the three previous cases. The amplification curves present the same shape as for the $m = 2$ case with a maximum when k tends to zero. The dynamics leading to energy growth always consists of the Orr mechanism. The dominant input structure is the spiralling vorticity sheets that uncoil due to the differential rotation. No transient resonance mechanism has been found, as could have been expected by considering the large damping rate of the Kelvin waves (Fabre *et al.* 2006). This phenomenon is valid for all $m > 2$. While energy growth is observed, these cases are of limited interest as they are exceedingly unlikely to prevail over the responses corresponding to the first three azimuthal wavenumbers.

4. Discussion

The results obtained in the present study show a noticeable similarity between the amplification curves for the different azimuthal wavenumbers considered here ($m \in [0, 10]$): the energy gain is maximum for $k = 0$ and decreases as k increases. This theoretical lack of intrinsic axial wavelength selection raises questions regarding the use of the present results to predict the response of the vortex in real-life conditions.

At this stage, we wish to underline that the interpretation of the amplification curves must be undertaken carefully. If one wants to predict the selection of a particular wavelength, a direct and hasty extrapolation of the results presented in this paper can prove completely erroneous when compared to experiments without any caution. Thus, taking the most amplified (k, m) modes corresponding to $m = 0$ and k tending to zero, it could be tempting to predict the systematic and dominant occurrence of very large axisymmetric vortex rings at the outer periphery of the vortex, as presented in § 3.1. But this conclusion, if applied to realistic experiments or observations, must be balanced by taking into account the departure of the experimental conditions from the hypotheses that define the framework of the present analysis. It concerns the unbounded character of the flow, the spectral content of the external forcing and the influence of the nonlinearities. These points are discussed further in this section.

4.1. *Bounded vs unbounded flows*

First, the largest amplifications are obtained in the limit of infinite wavelengths ($k \to 0$) for every azimuthal wavenumber m, suggesting that the response of the vortex should be systematically quasi-two-dimensional, at least for $m > 0$, and involve very large structures. But it must be kept in mind that the input structures triggering the vortex response (azimuthal streaks for $m = 0$ and axial vorticity spirals for $m > 0$) are localized radially further away from the vortex axis when k decreases, eventually extending to infinity for $k \to 0$. This singular behaviour questions the validity of the unbounded flow hypothesis that is implicitly made in the present formulation. It is expected that the predictions concerning the long-wave response of the vortex put forward in the previous sections will be distorted by the presence of physical boundaries at finite distance such as the sidewalls of the wind tunnel, or by taking into account flow features ignored in the present model such as other vortices. The present study found no intrinsic wavelength selection by the vortex and the process of wavelength selection is extrinsic and therefore case-dependent.

Nevertheless, the present results show that the physical mechanisms of growth involved in the response of the vortex systematically favour the structures with the largest axial wavelength, admissible as long as their radial extent does not exceed the limit of representativeness of the vortex flow model used here. We then expect the present results to be relevant above a critical axial wavenumber $k_c \sim 2\pi/r_c$ corresponding to a characteristic radial extent r_c above which the vortex flow model used here significantly departs from real-life conditions.

This discussion can also be supplemented, to a lesser extent, by the validity of the infinite time limit required to reach theoretically a statistical steady state in the present formulation. The input structures that are favoured in the $k \to 0$ limit correspond to infinitely slowly growing disturbances (Antkowiak & Brancher 2004; PH06; AB07). These perturbations thus may not have enough time to grow significantly in finite-time experiments. This is a second source of distortion for the large-wavelength results presented here. If the flow develops on a short or medium time scale, one can expect the selection of finite-time optimal perturbations which can be radically different from the structures predicted here for an infinite time horizon.

4.2. *Initial turbulence vs. continuous white noise*

The linear evolution of perturbations of a vortex flow is formally given by the general solution of the governing equation (2.1*a*) which has two components: the homogeneous solution which describes the evolution of initial conditions and the particular solution which represents the long-time response of the flow to a continuous external forcing. As mentioned by Schmid (2007), both parts are complementary and fully describe the general dynamics of small perturbations.

The studies of perturbed vortices generally focus on the former point, the evolution of *initial conditions*, such as temporal modal stability analyses (see Fabre *et al.* 2006 for the Lamb–Oseen vortex), optimal perturbation analyses (Antkowiak & Brancher 2004; PH06; AB07) or theoretical and numerical investigations of the response of vortices to initially injected turbulence (Melander & Hussain 1993; Risso, Corjon & Stoessel 1997; Miyazaki & Hunt 2000; Takahashi, Ishii & Miyazaki 2005; Marshall & Beninati 2005). More particularly in the latter case, the objective is to understand how the vortex immersed in an initial turbulent field responds to this perturbation and how in return the initial turbulence is affected by the presence of the vortex and the associated shear and rotation which are known to drastically alter the statistics of turbulence on a short time scale.

By contrast with these studies, the approach adopted in the present paper is quite different, as it focuses on the long-time response of the vortex when subjected to a *continuous external forcing*. This corresponds formally to the study of the particular solution of equation (2.1*a*) as stated by Schmid (2007). Physically this particular solution provides a model for a receptivity process, where the external forcing may represent either free stream turbulence, wall roughness or other non-smooth geometries, body forces or even neglected terms such as nonlinearities. This forcing can also be linked to the deviation from the model base flow, like the presence of other vortices far away or the boundary-layer perturbations generated at the sidewalls of the wind tunnel. In that context of receptivity analysis, the continuous forcing used in this study is chosen as generic and unbiased as possible in the form of white noise. Being equally distributed in space allows all possible regions of the flow to be excited and no specific wavelength or frequency to be favoured. Thus, if the wavelength selection is case-dependent (on the dominant wavelengths or frequencies of the external forcing in real-life conditions for instance†, see the preceding section), the quantification of the amplification is nevertheless a measure of the intrinsic transfer function of the Lamb–Oseen vortex, and reveals the intrinsic mechanisms that are favoured by the flow. Here it is shown that the largest response is observed in forcing scenarios that convert perturbations in the form of azimuthal velocity streaks into intense azimuthal vortex rings (for the axisymmetric part of the flow), and perturbations in the form of spiralling axial vorticity sheets outside the vortex into large bending ($m = 1$) and deformation waves ($m > 1$) within the vortex. It is noteworthy that these mechanisms are similar to the ones uncovered by non-modal studies of the initial-condition problem such as optimal perturbation analyses (PH06; AB07) and are consistent with the numerical simulations of the interaction of a vortex with an initial turbulent field. This suggests that such mechanisms are robust and fundamental to the dynamics of perturbed vortices. It is expected that they are potentially active whatever the details of the vortex flow and the perturbations considered.

4.3. *Validity of the linear approach*

This work has been conducted within the linear approximation and it is important to assess how the results obtained here are affected by the nonlinearities. The physical mechanisms of transient energy amplification considered here and in the studies of PH06 and AB07 are linear. As argued by Miyazaki & Hunt (2000), linear analysis correctly describes these processes or at least their initial development, while the nonlinearities affect the further evolution of individual structures. This point is currently under investigation via direct numerical simulations of the nonlinear evolution of the optimal perturbations. Preliminary results for the $m = 0$ case show that the azimuthal vorticity rings of the output structure are self-advected away from the vortex axis, carrying the streaks of high azimuthal velocity of the forcing structure. Due to the conservation of angular momentum, the intensity of the streaks decreases as the structures move radially outwards. Thus, the axisymmetric mechanism of energy growth is progressively damped by the nonlinearities. In the case of a maintained

† More precisely, as mentioned by one referee, a forcing of the form of a realistic turbulent signal would inject very low-amplitude perturbations at large scales $k \to 0$, and therefore a peak is expected at some finite wavelength in the response variance for each m. This wavelength selection will depend on the spectral content of the azimuthal Fourier decomposition of the turbulent signal, which might be highly sensitive to the particularities of the experimental environment in the long-wave limit.

forcing, this nonlinear damping effect is expected to be of minor importance as the streaks of azimuthal velocity would be statistically regenerated continuously.

Concerning the external forcing from a more general perturbation field, the nonlinear development of the flow should be considered for all wavenumbers simultaneously. Numerical simulations including a continuous forcing would be of great interest in order to show how the amplification factors obtained here are affected by the nonlinear effects (i.e. saturation). For the case of a transient forcing induced by an initially homogeneous isotropic turbulence, Takahashi *et al.* (2005) performed such analysis. The departure from the linear regime occurs when the bending wave growing in the core reaches a finite amplitude. They measured the impact on nonlinearities quantitatively through the time dependence of the axisymmetric axial correlation function. Its temporal growth was observed to be proportional to t, contrary to linear RDT analyses where a quadratic time dependence was found (Miyazaki & Hunt 2000). Thus, the nonlinear terms tend to limit the energy growth and a similar saturation is expected for any generic random forcing.

5. Conclusions

The goal of the present study is to analyse the dynamics of the Lamb–Oseen vortex when continuously forced by a random excitation. Considering the existence of transient growth in vortices when subjected to specific perturbations, this work aims to determine if the optimal perturbations found by Antkowiak & Brancher (2004, 2007) and Pradeep & Hussain (2006) could naturally emerge from background noise. For this purpose, the linear Navier–Stokes equations are continuously forced with Gaussian white noise so as to mimic any perturbations occurring in real transitioning flows. We then looked at the large-time statistical response of the vortex and at the coherent structures participating in its excitation. Not only does this method allow the energy gain of the system to be quantified but also finds and orders the coherent input (resp. output) structures according to their contribution to the excitation (resp. variance or response) of the flow.

For all azimuthal wavenumbers investigated, energy amplification is always observed, but when $m > 2$ the levels reached are too small compared to those obtained for smaller values of m to be significant. Compared to the optimal perturbation analysis, the levels of amplification obtained here are always higher since they correspond to energy growth resulting from a continuous noise input and not from a single initial condition. This difference in the value of the gain is particularly marked when the optimal perturbation evolves on a short time scale. In such cases, the sub-optimal perturbations should be considered as they participate equally in the vortex response. This point is one advantage of the stochastic forcing approach. The optimal perturbation analysis classically focuses on the most amplified disturbance and can sometimes miss some transitional scenarios. This is what we observe for the $m = 2$ case where no prevailing mechanism has been found to dominate the vortex dynamics.

Focusing on the physical mechanisms leading to energy growth, the scenarios leading to the vortex excitation identified by Antkowiak & Brancher (2004, AB07) and PH06 are recovered. This study confirms that the optimal perturbations can be activated naturally by the background noise present in uncontrolled conditions.

In the axisymmetric case, the mechanism called ‘anti-lift-up’ by AB07 consists of the emergence at the vortex periphery of strong tori of azimuthal vorticity fed by the azimuthal velocity streaks of the forcing structure. This scenario is a theoretical

counterpart to the observation of the recurrent development of vortex rings at the periphery of vortices when submerged in an ambient turbulence (Melander & Hussain 1993; Risso *et al.* 1997; Takahashi *et al.* 2005).

For helical perturbations, the excitation of the vortex is explained by a transient resonance phenomenon. The dominant forcing structure is composed of two left-handed entangled vorticity sheets located in the quasi-potential region of the flow. As time evolves, they progressively uncoil under the base-flow differential rotation and trigger the appearance of a Kelvin wave through a process combining induction effects and the Orr mechanism. The emerging Kelvin mode depends on the axial wavenumber as the selection is based both on a minimization of the wave damping rate and a concordance between the pulsations of both the mode and the vorticity spirals. At large wavelengths where the gain is maximal, the displacement mode of Fabre *et al.* (2006) is preferentially excited. The emergence of the displacement wave under the influence of a maintained background noise is thus an interesting candidate for the vortex meandering observed in the experiments (Baker *et al.* 1974; Devenport *et al.* 1996).

This mechanism of resonance originating from a localized spiralling vorticity disturbance also occurs for $m = 2$ perturbations with the emergence of the flattening wave. But it is in competition with other disturbances experiencing transient growth. The disentanglement of the vorticity spirals via the base-flow differential rotation leads to energy amplifications as large as those derived from the flattening mode resonance. The existence of sub-optimal perturbations growing on a longer time scale than the optimal one is put forward to explain the discrepancy between the results obtained here and those of PH06. This point is to be confirmed. It will be investigated in the near future with the computation of the sub-optimal perturbations of the Lamb–Oseen vortex for $m = 2$. For larger wavenumbers, the Orr mechanism becomes the dominant process of energy amplification from a continuous random excitation of the vortex.

Finally, the approach taken here answers the questions raised by the results of the optimal perturbation studies of Antkowiak & Brancher (2004), AB07 and PH06. This work demonstrates both analyses to be complementary. Such tools may be applied to asymptotically stable flows whose dynamical operator is non-normal in order to find an eventual transient mechanism. For example, Joly, Fontane & Chassaing (2005) recently showed that low-density vortices were insensitive to the Rayleigh–Taylor instability. Since the corresponding dynamical operator does not commute with its Hermitian transpose, non-modal stability analysis (both initial value and stochastic forcing formulations) should be conducted.

This work was supported by the European Community in the framework of the FAR-WAKE project under grant number AST4-CT-2005-012238 and the French National Research Agency as part of the VORTEX project.

REFERENCES

Antkowiak, A. 2005 Dynamique aux temps courts d'un tourbillon isolé. PhD thesis, Université Paul Sabatier (UPS), Toulouse, France.

Antkowiak, A. & Brancher, P. 2004 Transient energy growth for the Lamb-Oseen vortex. *Phys. Fluids* **16**, L1–L4.

Antkowiak, A. & Brancher, P. 2007 On vortex rings around vortices: an optimal mechanism. *J. Fluid Mech.* **578**, 295–304.

Baker, G. R., Barker, S. J., Bofah, K. K. & Saffman, P. G. 1974 Laser anemometer measurements of trailing vortices in water. *J. Fluid Mech.* **65**, 325–336.

Bamieh, B. & Dahleh, M. 2001 Energy amplification in channel flows with stochastic excitation. *Phys. Fluids* **13**, 3258–3269.

Billant, P., Brancher, P. & Chomaz, J. M. 1999 Three-dimensional stability of a vortex pair. *Phys. Fluids* **11**, 2069–2077.

Butler, K. M. & Farrell, B. F. 1992 Three-dimensional optimal perturbations in viscous shear flow. *Phys. Fluids* A **4**, 1637–1650.

Butler, K. M. & Farrell, B. F. 1993 Optimal perturbations and streak spacing in wall-bounded turbulent shear flow. *Phys. Fluids* A **5**, 774–777.

Corbett, P. & Bottaro, A. 2001 Optimal linear growth in swept bounday layers. *J. Fluid Mech.* **435**, 1–23.

Crow, S. C. 1970 Stability theory for a pair of trailing vortices. *AIAA J.* **8**, 2172–2179.

Devenport, W. J., Rife, M. C., Liapis, S. I. & Follin, G. J. 1996 The structure and development of a wing-tip vortex. *J. Fluid Mech.* **312**, 60–106.

Fabre, D. & Jacquin, L. 2004 Viscous instabilities in trailing vortices at large swirl numbers. *J. Fluid Mech.* **500**, 239–262.

Fabre, D., Sipp, D. & Jacquin, L. 2006 Kelvin waves and the singular modes of the Lamb-Oseen vortex. *J. Fluid Mech.* **551**, 235–274.

Farrell, B. F. & Ioannou, P. J. 1993*a* Optimal excitation of three-dimensionnal perturbations in viscous constant shear flow. *Phys. Fluids* A **5**, 1390–1400.

Farrell, B. F. & Ioannou, P. J. 1993*b* Stochastic forcing of the linearized Navier-Stokes equations. *Phys. Fluids* A **5**, 2600–2609.

Farrell, B. F. & Ioannou, P. J. 1994 Variance maintained by stochasting forcing of non-normal dynamical systems associated with linearly stable shear flows. *Phys. Rev. Lett.* **72**, 1188–1191.

Hoepffner, J. 2006 Stability and control of shear flows subject to stochastic excitations. PhD thesis, R. Inst. Tech. (KTH), Stockholm, Sweden.

Joly, L., Fontane, J. & Chassaing, P. 2005 The Rayleigh-Taylor instability of two-dimensional high-density vortices. *J. Fluid Mech.* **537**, 415–431.

Jovanovic, M. & Bamieh, B. 2005 Componentwise energy amplification in channel flows. *J. Fluid Mech.* **534**, 145–183.

Leweke, T. & Williamson, C. H. K. 1998 Cooperative elliptic instability of a vortex pair. *J. Fluid Mech.* **360**, 85–119.

Marshall, J. S. & Beninati, M. L. 2005 External turbulence interaction with a columnar vortex. *J. Fluid Mech.* **540**, 221–245.

Melander, M. V. & Hussain, F. 1993 Coupling between a coherent structure and fine-scale turbulence. *Phys. Rev.* E **48**, 2669–2689.

Miyazaki, T. & Hunt, J. 2000 Linear and non-linear interactions between a columnar vortex and external turbulence. *J. Fluid Mech.* **402**, 349–378.

Moore, D. W. & Saffman, P. G. 1975 The instability of a straigth vortex filament in a strain field. *Proc. R. Soc. Lond.* A **346**, 413–425.

Nolan, D.S. & Farrell, B. F. 1999 The intensification of two-dimensional swirling flows by stochastic asymmetric forcing. *J. Atmos. Sci.* **56**, 3937–3962.

Orr, W. M. 1907*a* The stability or instability of the steady motions of a perfect liquid and of a viscous liquid. part 1: A perfect liquid. *Proc. R. Irish Acad.* **27**, 9–68.

Orr, W. M. 1907*b* The stability or instability of the steady motions of a perfect liquid and of a viscous liquid. part 2: A viscous liquid. *Proc. R. Irish Acad.* **27**, 69–138.

Pradeep, D. S. & Hussain, F. 2006 Transient growth of perturbations in a vortex column. *J. Fluid Mech.* **550**, 251–288.

Reddy, S. C. & Henningson, D. S. 1993 Energy growth in viscous channel flows. *J. Fluid Mech.* **252**, 209–238.

Reddy, S. C., Schmid, P. J. & Henningson, D. S. 1993 Pseudospectra of the Orr-Sommerfeld operator. *SIAM J. Appl. Maths* **53**, 15–47.

Risso, F., Corjon, A. & Stoessel, A. 1997 Direct numerical simulations of wake vortices in intense homogeneous turbulence. *AIAA J.* **35**, 1030–1040.

Schmid, P. J. 2007 Nonmodal stability theory. *Annu. Rev. Fluid Mech.* **39**, 129–162.

Takahashi, N., Ishii, H. & Miyazaki, T. 2005 The influence of turbulence on a columnar vortex. *Phys. Fluids* **17**, 035105.

Trefethen, L. N., Trefethen, A. E., Reddy, S. C. & Driscoll, T. A. 1993 Hydrodynamic stability without eigenvalues. *Science* **261**, 578–584.

Tsai, C. Y. & Widnall, S. E. 1976 The stability of short waves on a straight vortex filament in a weak externally imposed starin field. *J. Fluid Mech.* **73**, 721–733.

Weideman, J. A. C. & Reddy, S. C. 2000 A matlab differentiation matrix suite. *ACM Trans. Math. Soft.* **26**, 465–519.

Whitaker, J. S. & Sardeshmukh, P. D. 1998 A linear theory of extratropical synoptic eddy statistics. *J. Atmos. Sci.* **55**, 238–258.

Zhou, K., Doyle, J. & Glover, K. 1995 *Robust and Optimal Control*, 1st edn. Prentice Hall.